PLANT SCIENCES

Leaf economics fundamentals explained by optimality principles

Han Wang[1]*, I. Colin Prentice[1,2,3], Ian J. Wright[3,4], David I. Warton[5], Shengchao Qiao[1], Xiangtao Xu[6], Jian Zhou[1], Kihachiro Kikuzawa[7], Nils Chr. Stenseth[1,8]

The life span of leaves increases with their mass per unit area (LMA). It is unclear why. Here, we show that this empirical generalization (the foundation of the worldwide leaf economics spectrum) is a consequence of natural selection, maximizing average net carbon gain over the leaf life cycle. Analyzing two large leaf trait datasets, we show that evergreen and deciduous species with diverse construction costs (assumed proportional to LMA) are selected by light, temperature, and growing-season length in different, but predictable, ways. We quantitatively explain the observed divergent latitudinal trends in evergreen and deciduous LMA and show how local distributions of LMA arise by selection under different environmental conditions acting on the species pool. These results illustrate how optimality principles can underpin a new theory for plant geography and terrestrial carbon dynamics.

INTRODUCTION

All life on Earth is continuously subject to selective pressures imposed by environmental conditions. The rapidly changing environment of the Anthropocene is modifying the selective pressures on plant traits that play key roles in the terrestrial carbon cycle, with largely unknown consequences. Plant leaves are subject to strong selection for economic efficiency in carbon uptake (*1*, *2*). The leaf economics spectrum (LES), describing observed relationships among different leaf traits, has at its core the fact that plants with thicker and/or denser leaves (high leaf mass per area, LMA) have longer life spans (high leaf longevity, LL) (*3*, *4*). Together, these traits influence carbon cycling in terrestrial ecosystems by determining the carbon requirement for leaf construction and turnover. Understanding the LES is a major goal in plant functional ecology and is necessary for more robust modeling of the global carbon cycle and its responses and feedbacks to changes in atmospheric CO_2 and climate (*5*–*7*).

LL and LMA vary several hundred-fold across vascular plants and up to 10-fold among cooccurring species (*3*, *8*). Large-scale trends in both traits strongly suggest the existence of a common organizing principle (*9*–*12*). However, the environmental controls on variation in LL and LMA remain to be clarified (*13*), as do the distinct responses of the deciduous and evergreen leaf habits (*13*). In particular, why do the leaves of deciduous trees and shrubs tend to become thinner (as their life span declines) poleward, while those of evergreen species become thicker (*14*) and longer-lived (*15*)?

Recent research has shown that the principle of eco-evolutionary optimality, invoking the power of natural selection to eliminate uncompetitive trait combinations, can predict a priori the observed patterns of relationship among plant traits and between traits and environment (*16*). The increasing availability of large plant trait datasets allows independent, quantitative assessment of such predictions (*17*). This combined data- and theory-driven approach holds promise for better understanding of ecological processes and improvement of land-surface models (*16*, *18*). However, because of the unknown effects of species adaptation (on an evolutionary time scale) on trait variations, much research has focused on physiological traits, such as photosynthetic capacity, that can acclimate even within the life cycle of a single leaf following seasonal cues (*19*, *20*). LMA and LL show more muted intraspecific responses to temporal changes and geographic gradients in environmental factors, suggesting a key role of adaptation in mediating the shifts of community-mean trait values (*21*). Moreover, eco-evolutionary optimality hypotheses typically predict a single value for a given trait, representing a site-specific optimum. This approach provides no information on within-site functional diversity and, therefore, adds uncertainty in predicting the function and resilience of diverse ecosystems under environmental change.

Here, we propose a theory based on eco-evolutionary optimality that predicts how the LES for woody plant species depends on environmental variables. We test our predictions using two large, independent leaf trait datasets. We use the theory to explain why deciduous and evergreen leaves show opposite latitudinal trends in LMA, and how site-specific functional diversity of LMA is shaped jointly by environmental selection and evolutionary history.

We start by developing a unified optimality framework for the LES. First, we consider the relationship between LMA and LL that maximizes the leaf life cycle (LC) average net carbon gain, i.e., net photosynthesis minus the associated (amortized) tissue construction costs (*22*). This relationship depends on the rate of photosynthetic decline with leaf age (*23*). Second, the aging rate increases in proportion to the leaf's initial photosynthetic capacity, as measured by the maximum rate of carboxylation at a standard temperature of 25°C (V_{cmax25}), and decreases in proportion to LMA (*23*). Third,

[1]Ministry of Education Key Laboratory for Earth System Modeling, Department of Earth System Science, Tsinghua University, Beijing 100084, China. [2]Georgina Mace Centre for the Living Planet, Department of Life Sciences, Imperial College London, Silwood Park Campus, Buckhurst Road, Ascot SL5 7PY, UK. [3]School of Natural Sciences, Macquarie University, North Ryde, NSW 2109, Australia. [4]Hawkesbury Institute for the Environment, Western Sydney University, Penrith 2751, Australia. [5]School of Mathematics and Statistics and Evolution and Ecology Research Center, UNSW Sydney, Sidney, NSW 2052, Australia. [6]Ecology and Evolutionary Biology, Cornell University, E139 Corson Hall, Ithaca, NY 14850, USA. [7]Laboratory of Plant Ecology, Ishikawa Prefectural University, Nonoichi, Ishikawa 921-8836, Japan. [8]Centre for Ecological and Evolutionary Synthesis (CEES), Department of Biosciences, University of Oslo, P.O. Box 1066 Blindern, Oslo NO-0316, Norway.
*Corresponding author. Email: wang_han@tsinghua.edu.cn

photosynthetic capacity itself is optimized to the physical environment, following the coordination hypothesis (*24*–*26*). We account for the key distinction between deciduous and evergreen species: The LC is equal to LL for evergreen species but to 365 days for deciduous species (whose LL is strongly constrained by growing-season length). We obtain the following relationships between optimal LL and LMA in evergreen and deciduous leaves (see Materials and Methods for derivations)

$$\mathrm{LL_{ev}} = \frac{\mathrm{LMA}}{A_0}\sqrt{\frac{2\,u\,h_T\,m_c\,C_c}{f}} \quad (1)$$

$$\mathrm{LL_{de}} = \frac{\mathrm{LMA}}{A_0}(u\,h_T\,m_c) = 365f \quad (2)$$

where subscripts "ev" and "de" denote evergreen and deciduous species, respectively; A_0 is the leaf's initial photosynthetic rate; f is the growing-season length, as a fraction of the year; and u is a constant that relates the aging rate to LMA and photosynthetic capacity. C_c is a multiplier for the plant-level total carbon costs of leaf construction, including all required investments in constructing and maintaining supporting tissues. This definition is more explicit than the original one provided by Kikuzawa (*22*). By linking the whole plant-level cost to LMA, we can now estimate C_c from empirical observations (see detailed information in Materials and Methods). h_T is the Arrhenius function relating V_{cmax} to temperature (T), equal to unity when T = 25°C; and m_c is the ratio of the Rubisco-limited photosynthetic rate to V_{cmax}, which is a function of the intercellular CO_2 partial pressure, the photorespiratory compensation point, and the affinity of Rubisco for CO_2 versus O_2. The coordination hypothesis predicts that A_0 is proportional to the photosynthetic photon flux density (PPFD) absorbed by the leaf. This theory predicts the existence of a spectrum of values of both quantities, from low LMA and LL to high LMA and LL, resulting in equal rates of net carbon gain (see Materials and Methods), thus providing a formal mathematical expression for the foundational relationship underlying the LES.

RESULTS AND DISCUSSION

For evergreens, the optimal LL in a given environment is proportional to LMA and inversely proportional to absorbed PPFD and the square root of growing-season length. We show here (Fig. 1, A to C, and table S1) that these predictions are close to the corresponding partial effects independently inferred from a multiple regression fitted to the measurements on evergreen species in the Glopnet dataset (*3*), which provides the largest available worldwide compilation of paired data on LMA and LL. The regression for evergreen species captures 42% of the variation in LL. Globally, the fitted relationship of evergreen LL to LMA—with other environmental predictors included—is a proportionality (log-log slope ≈ 1), as predicted (tables S1 and S2), and consistent with (*12*). Standardized major axis (SMA) regression, without environmental covariates, indicates a steeper overall slope of LL against LMA (log-log slope = 1.41). However, analysis of within-site relationships between LL and LMA shows that log-log SMA slopes > 1 are particularly a feature of denser canopies (fig. S1). This might reflect sampling bias, whereby leaves are systematically sampled from lower light conditions in more dense vegetation (*27*), or possibly the effect of "time-discounting" (*1*), whereby the average light conditions experienced by a leaf diminish more rapidly over time in denser canopies. The observed relationship of LL to PPFD is negative as predicted, and the relationship of LL to growing-season length is also negative ($P < 0.1$) as predicted, both with theoretical slope coefficients similar in magnitude to fitted values. For deciduous species, in addition to the optimality criterion, $\mathrm{LL_{de}}$ is assumed to be tightly constrained by growing-season length. Among the deciduous species in Glopnet, growing-season length is indeed nearly proportional to LL (0.99 ± 0.06, 1 SE) and explains about 70% of the observed variation in LL (Fig. 1D and table S1).

To quantify the environmental dependencies of LMA, we consider how environmental selection interacts with other physiological or evolutionary constraints. For evergreens, we consider the prior probability distributions of LMA and LL (fig. S2) as an evolutionary constraint. The principle is illustrated in fig. S3, where straight lines in the log-log plot of LL versus LMA— representing the optimal LES for sites in different environments—intersect log-normal distributions of both traits. The resulting predicted sensitivities of evergreen LMA to PPFD are only half those for deciduous LMA (see Materials and Methods). For growing-season length and temperature, they are only a quarter of those for deciduous LMA.

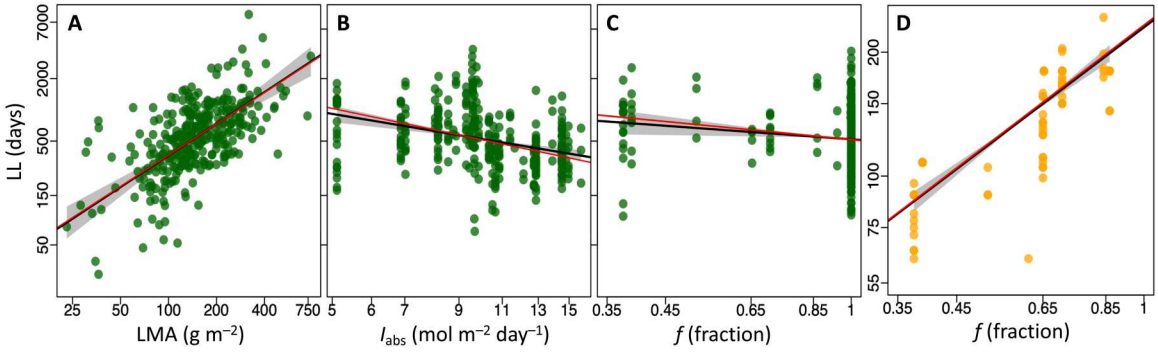

Fig. 1. Partial residual plots for observed leaf longevity (LL) against explanatory variables. (**A**) LMA, leaf mass per area. (**B**) I_{abs}, site-mean leaf-absorbed PPFD. (**C** and **D**) *f*, fractional growing-season length. Predicted: red. Fitted: black, with 95% confidence intervals. Evergreen: green. Deciduous: orange. All axes are log-scaled. Data from Glopnet (*3*).

Last, for both deciduous and evergreen species, environmental aridity is expected (and found) to impose an additional physiological constraint on LMA, probably due to a requirement for physically robust leaves to maintain turgor at low leaf water potentials (*28*) and/or for thermal buffering at high leaf temperatures (*29*).

These predictions are broadly supported by analysis of data in the China Plant Trait Database (CPTD) (*30*), which provides site climatology with high spatial resolution (1 km), a larger LMA dataset than Glopnet for temperate and boreal deciduous species, many more observations for deciduous species, and data from more than three times as many sites. Growing-season PPFD, temperature, and an index of plant-available moisture (see Materials and Methods) all significantly influenced the LMA of evergreen species (Fig. 2, A to C, and table S3). The predictive power of this relationship was limited (13%), however, presumably because environmental predictors alone can only explain part of the variation in LMA, while additional variation is expected to be driven by variation in LL, and the effect of growing-season length could not be unequivocally disentangled from that of PPFD due to multicollinearity. The first two principal components accounted for 94% of variance in PPFD, temperature, moisture, and growing-season length (fig. S4); when growing-season length was included as a predictor, the effect of PPFD (variance inflation factor = 3.6) became nonsignificant (table S3). Growing-season length was nonetheless a significant predictor of the residual variation in evergreen LMA, explaining a further 3% of variance in the residuals from the model based on PPFD, temperature, and moisture (Fig. 2D and table S3). These same four predictors accounted for over half the variation in LMA among deciduous species in the CPTD (Fig. 2, E to H, and table S3), where growing-season length is expected to largely determine LL and to be proportional to LMA, as observed. The confidence intervals of the fitted coefficients for PPFD, temperature, and growing-season length all included the predicted values for both evergreen and deciduous species, and the expected negative effect of moisture on LMA was found in both evergreen and deciduous species (Fig. 2, C and G, and tables S3 and S4).

This theory accounts for the contrasting latitudinal patterns in LMA between deciduous and evergreen species (Fig. 3 and fig. S5) (*31*). The effect of increasing temperature alone toward the equator on LMA is negative for both leaf types and stronger for deciduous leaves. According to our theory, this response of LMA to growth temperature is attributed to the thermal acclimation of carboxylation capacity (*23*, *26*). At higher temperatures, less investment in photosynthetic enzymes (i.e., lower carboxylation capacity when measured at standard temperature) is needed to produce a unit of photosynthate, which, according to the empirical relationship expressed by Eq. 12, leads to slower leaf aging at any given LMA. In deciduous species, this influence of temperature, however, is outweighed by the effects of increasing growing-season PPFD and length, both of which favor increased LMA (*32*).

The theory could be extended to consider variations in the cost of nutrient acquisition associated with below-ground microbial processes. Mass balance dictates that community nitrogen demand (to support leaf turnover) cannot exceed supply. In high latitudes where nitrogen is commonly limiting to plant growth and soil mineralization is slow, building new leaves may be more expensive than in warmer climates (*33*). Consistent with this idea, the multiplier C_c estimated at individual sites increases toward the poles (fig. S6). Higher C_c, in turn, predicts still greater LMA (fig. S7). Our theory therefore could lead to a qualitative explanation for why less-fertile soils favor species with higher LMA (*9*). The theory also provides a step forward toward predicting biogeographic distributions of evergreen and deciduous species as a result of the competition between average net carbon gain for the two strategies, taking into account environmental influences on C_c.

To address the functional diversity of LMA, we hypothesize that site-mean LMA should be predicted at the mean of the distribution

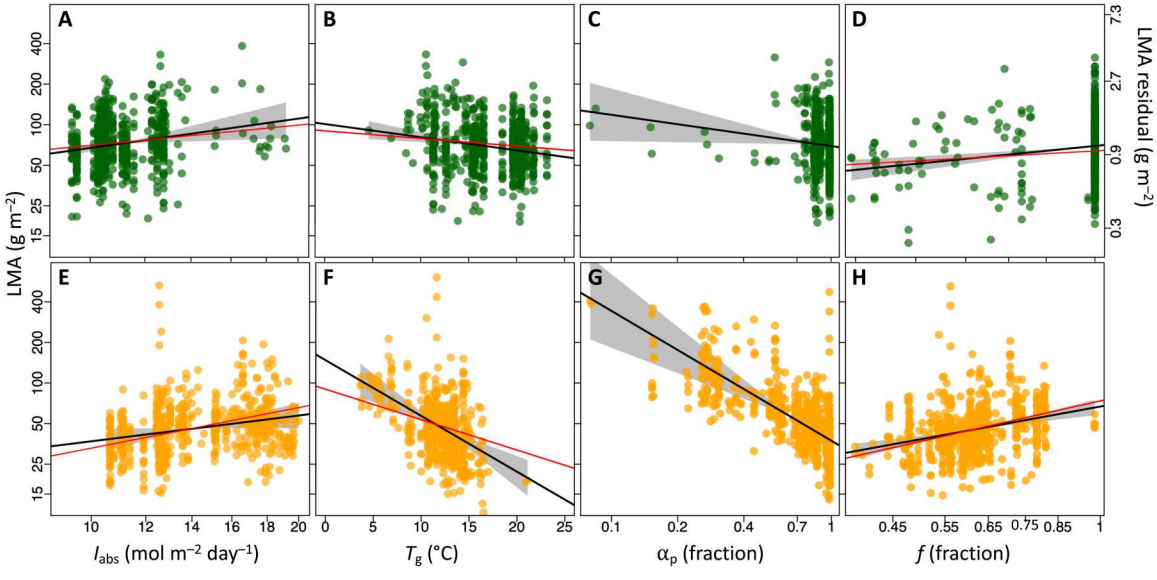

Fig. 2. Partial residual plots for observed LMA against environmental variables. (**A** and **E**) I_{abs}, site-mean leaf-absorbed photosynthetic PPFD. (**B** and **F**) T_g, mean growing-season temperature. (**C** and **G**) α_p, moisture index. (**D** and **H**) f, fractional growing-season length. Predicted: red. Fitted: black, with 95% confidence intervals. Evergreen: green. Deciduous: orange. All axes except T_g are log-scaled. Data from the extended CPTD (*30*, *40*).

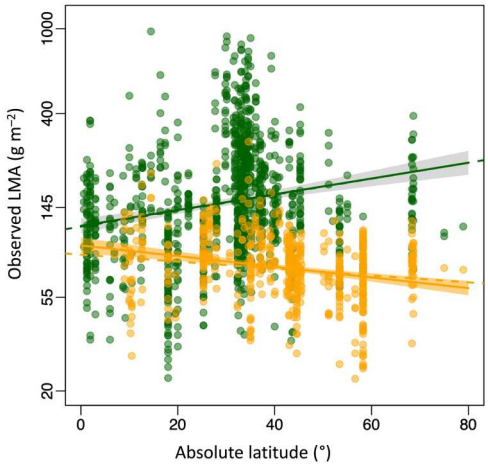

Fig. 3. Observed and predicted trends of LMA from tropical to polar regions. Evergreen: green; deciduous: orange. Solid lines, regressions with 95% confidence intervals. Dashed lines: theoretical predictions. Data from Glopnet (*3*).

formed by the intersection of the predicted lines with the prior distribution based on the global species pool (fig. S3). We fitted independent log-normal distributions of LMA and LL based on Glopnet data and imposed Eq. 1 as a constraint. This method successfully predicted within-community LMA distributions in evergreen temperate forests, tropical rain forests, and woodlands (Fig. 4). The

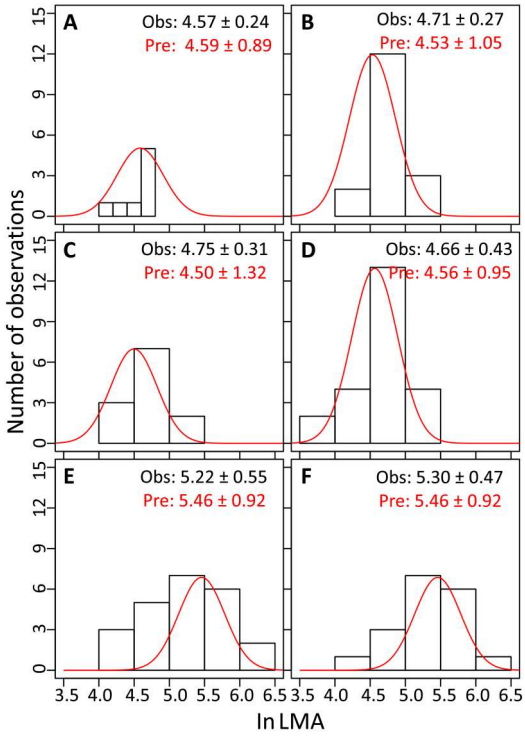

Fig. 4. Observed and predicted within-site distributions of LMA. (**A** and **B**) Temperate forests. (**C** and **D**) Tropical rain forests. (**E** and **F**) Woodlands. Means and SE of observed (Obs) and predicted (Pre) distributions are shown. Predicted distributions (red curves) are scaled in height to match observed distributions. Data from Glopnet (*3*). Sites with the largest sample sizes were selected. See detailed information in table S5.

community-mean LMA values of temperate forests and tropical rain forests are close to the global mean value of LMA derived from the Glopnet dataset. They are similar because growth temperature and growing-season PPFD and duration are positively correlated but have opposite effects on LMA. The community-mean LMA of woodlands (Fig. 4, E and F) however shifts to the right of the global mean, because of the ecophysiological constraint imposed by aridity.

Leaf-level maximization of life cycle average net carbon gain provides a quantitative eco-evolutionary explanation for the existence of the LES and for observed, systematic variations with environment of the relationship between LMA and LL that is fundamental to the LES. Like other optimality-based explanations for global patterns, the theory is silent on the physiological and anatomical mechanisms by which leaves can be adapted to different environments, which may indeed be diverse. The resulting patterns are nonetheless key to understanding the biogeographical dimension of leaf economics. Unlike variations in physiological traits, these patterns are primarily determined by environmental selection among species rather than plasticity and genetic adaptation within species (*21*, *34*). However, plants do have some plasticity for LMA, as has been shown experimentally (*35*). Experimental effects on LMA include positive responses to PPFD, CO_2, aridity, and a negative response to growth temperature (*35*, *36*)—all in the same direction as predicted here but smaller in magnitude. Some uncertainties are inevitable in a global-scale quantitative empirical test, such as the representativeness of environmental conditions extracted from the gridded climatic products, sampling biases, and potential multicollinearity among environmental variables. More rigorous quantitative tests of predicted environmental effects on the LES will require both experimental studies and more systematic field surveys. Nonetheless, our analysis of available data broadly supports the predictions of the theory, which may serve as a key step toward a more comprehensive understanding of the adaptive value and competitive success of different plant strategies. The successful application of our theory in understanding the observed declining trend of nitrogen content in vegetation canopies confirms its promising role in addressing and predicting the dynamics of the global carbon cycle under environmental change (*37*).

Plants have been subject to profound changes in climate during their evolutionary history. Large and, sometimes, rapid changes in recent geological times have resulted in repeated large-scale reassortments of species and consequent major changes in community composition (*38*, *39*). Current anthropogenic environmental changes are adding to the forces shaping plant communities, in ways that remain only partly understood (*7*). On the basis of evolutionary thinking—taking into account the changing selective pressures imposed by changing environmental conditions—we suggest that optimality theory may serve not only to resolve the puzzles of global phytogeography but also to help to move plant functional ecology from empirical description to robust theoretical and predictive understanding (*16*).

MATERIALS AND METHODS

Leaf trait data

We tested our quantitative predictions with the woody plants represented in two nonoverlapping datasets: the Glopnet dataset (*3*) and the CPTD (*30*) augmented with data compiled by Geng *et al.*

(*40*) from alpine shrublands. Glopnet contains paired LMA and LL data for 326 evergreen and 179 deciduous species at 45 sites distributed globally. For deciduous plants, we focus here on those whose growing season is constrained by a cold winter; thus, tropical deciduous species that shed leaves in the dry season have been excluded from the analysis. Applying this filtering criterion, the Glopnet dataset contains data on LMA alone from 1225 evergreen and 98 deciduous species at 146 sites, distributed from 69°S to 40°N. The CPTD provides LMA data from 419 for evergreen and 398 deciduous species at 164 sites, spanning the range from alpine and boreal to tropical environments and from desert and steppe vegetation to woodlands and forests. Data in the CPTD were obtained using a consistent sampling strategy to ensure adequate representation of species in all strata.

Site climate data

We calculated site-specific bioclimatic variables from monthly temperature, precipitation, and sunshine hours with the Simple Process-Led Algorithms for Simulating Habitats (SPLASH) model (*41*). This model has been validated at both site and global scales (*41*) and has been extensively used to calculate bioclimatic variables. Defining the (thermal) growing season as the period when mean quasi-daily temperature (interpolated from monthly data) is above 0°C, we calculated the ratio of growing-season length to the number of days in the year and the mean values of temperature and PPFD during growing season, as estimates of site-mean f, T_g, and PPFD. A moisture index, defined as the ratio of estimated annual actual to potential evapotranspiration (denoted α_p), was also calculated using SPLASH. For the Glopnet dataset, time series monthly climate data for the period 1981 to 2010 were extracted for each site from Climate Research Unit data at a grid resolution of 0.5° (*42*). This 30-year period allowed us to estimate both climatological mean values and interannual variations of calculated bioclimatic variables. To account for the fact that the field-measured trait data reflect leaves developed at a range of irradiances at different levels in the canopy, we applied the approach used by Wang *et al.* (*43*) to estimate I_{abs} from the site-mean PPFD, with the help of leaf area index values extracted from Advanced Very-High-Resolution Radiometer (AVHRR) data at the same resolution and for the same time interval (*44*). The site-specific means and SDs of the calculated annual bioclimatic variables f, T_g, α_p, and I_{abs} allow an estimate of the reliability of bioclimatic variables, reflecting the uncertainties in the monthly climate inputs and the SPLASH calculations. For the extended CPTD, the database already contained f, T_g, α_p, and I_{abs}, and these data were used for our analyses. These bioclimatic data were also calculated using SPLASH but driven by higher-resolution (1 km) gridded climatological data interpolated from 1814 meteorological stations (China Meteorological Administration: 740 stations have observations from 1971 to 2000 and the rest from 1981 to 1990) using a three-dimensional thin-plate smoothing spline (ANUSPLIN version 4.36; Hancock and Hutchinson, 2006).

The optimality framework for leaf economics

The optimality model of leaf longevity (LL: day) proposed by Kikuzawa (*22*) rests on two assumptions. First, daily photosynthesis declines linearly from an initial maximum (denoted by A_0, g biomass m^{-2} day^{-1}) with increasing age. Second, LL maximizes the leaf's lifetime-average net carbon gain (accumulated daily photosynthesis averaged over LL minus the initial structural investment amortized over LL). Building on Kikuzawa's original work, we propose a new, unified optimality model for deciduous and evergreen species. For deciduous species, we extend the period for maximizing average net carbon gain from the LL to the whole LC (day), i.e., the period from the formation of a leaf until its replacement. LC is thus equal to LL for evergreen species but to 365 days for deciduous species. We further simplify the derivation by disregarding leaf maintenance respiration, as it is nearly proportional to photosynthetic capacity and represents only about 6% of leaf gross photosynthetic rate under standard environmental conditions (*43*, *45*, *46*). The daily net carbon gain (g) is then

$$g = (G - C_c\mathrm{LMA})/\mathrm{LC} \tag{3}$$

where G (g biomass m^{-2}) is the accumulated photosynthetic carbon gain over the life cycle. The initial structural investments are represented by the product of LMA and C_c, where LMA is leaf mass per area (g biomass m^{-2}), and C_c (>1, gC gC^{-1}) is the plant-level total construction cost, including all required investments in constructing and maintaining supporting leaf and nonleaf tissues, of a unit of leaf mass. G is represented differently for deciduous and evergreen species, since deciduous leaves can carry out photosynthesis during their whole life span, whereas evergreen leaves are inactive during the nongrowing season.

We use subscripts ev and de to distinguish evergreen and deciduous species. Thus, for evergreen plants

$$G_{ev} = \int_0^{LC} fA(t)\ dt \tag{4}$$

where $A(t) = A_0\ (1 - t/b)$ is the assimilation rate (g biomass m^{-2} day^{-1}) as a function of age (t, days), and b (days) is the (extrapolated) leaf age at which carbon assimilation would decline to zero. f is the proportion of the year that is favorable for growth (day day^{-1}). Since $LC_{ev} = LL_{ev}$, the integral in Eq. 4 is equal to $f\,A_0\ [LL_{ev} - (LL_{ev})^2/2b]$, and Eq. 3 collapses to Kikuzawa's model (*22*)

$$g_{ev} = fA_0(1 - \mathrm{LL}_{ev}/2b) - C_c\mathrm{LMA}/\mathrm{LL}_{ev} \tag{5}$$

hence,

$$\partial g_{ev}/\partial(\mathrm{LL}_{ev}) = -fA_0/2b + C_c\mathrm{LMA}/(\mathrm{LL}_{ev})^2 \tag{6}$$

Setting Eq. 6 to zero yields an expression for optimal LL_{ev} (days) in evergreen plants

$$\mathrm{LL}_{ev} = \sqrt{[(2b\ C_c\,\mathrm{LMA})/(f\ A_0)]} \tag{7}$$

For deciduous plants,

$$G_{de} = \int_0^{LC} A(t)\ dt = \int_0^{LL} A(t)\ dt \tag{8}$$

The integral in Eq. 8 equals $A_0\ [LL_{de} - (LL_{de})^2/2b]$ and thus

$$g_{de} = [A_0\ \mathrm{LL}_{de}(1 - \mathrm{LL}_{de}/2b) - C_c\ \mathrm{LMA}]/\mathrm{LC} \tag{9}$$

In deciduous species, LC = 365; thus,

$$\partial g_{de}/\partial(\mathrm{LL}_{de}) = A_0(1 - \mathrm{LL}_{de}/b)/365 \tag{10}$$

Setting Eq. 10 to zero yields a simple equation for optimal LL (days) in deciduous plants

$$\mathrm{LL}_{de} = b \tag{11}$$

We implemented the model of b proposed by Xu *et al.* (*23*) in the framework described above. Xu *et al.* demonstrated that b has a positive relationship with LMA, and a negative relationship to the V_{cmax25} (μmol C m^{-2} s^{-1}), with scaling coefficients close to 1 and −1, respectively. Therefore, b can be expressed as

$$b = u\ \mathrm{LMA}/(k_1\ k_2\ V_{cmax25}) \quad (12)$$

Here, $u \approx 768 \pm 71$ (dimensionless), estimated from a meta-analysis of data on 49 species across temperate and tropical biomes (*23*). The scaling factors are k_1 = 30 g biomass mol C^{-1} and k_2 = 0.0864 s mol C day^{-1} μmol^{-1} C.

The optimality model of leaf photosynthesis

The coordination hypothesis, supported by extensive field and experimental evidence (*26*, *47*), states that the maximum capacity of carboxylation at growth temperature ($V_{cmax.gt}$, μmol C m^{-2} s^{-1}) acclimates to the daytime environment so that the Rubisco-limited photosynthetic rate (A_C, μmol C m^{-2} s^{-1}) tends to be equal with the electron transport-limited rate (A_J, μmol C m^{-2} s^{-1}). In other words, $A_C = A_J$. This acclimation is optimal because it avoids investment in excess photosynthetic capacity while allowing full use of the available light (*24*, *25*). Combined with the standard biochemical model of photosynthesis (*45*), the coordination hypothesis predicts $V_{cmax.gt}$

$$A_C = V_{cmax.gt} m_c \quad (13)$$

$$A_J = \varphi_0 I_{abs} m \quad (14)$$

and

$$V_{cmax.gt} = \varphi_0 I_{abs} m/m_c \quad (15)$$

where

$$m = (c_i - \Gamma^*)/(c_i + 2\Gamma^*) \quad (16)$$

and

$$m_c = (c_i - \Gamma^*)/(c_i + K) \quad (17)$$

Here, ϕ_0 is the intrinsic quantum efficiency of photosynthesis (μmol C μmol^{-1} photon), which we assume to depend on temperature as described in (*48*). I_{abs} is the leaf-absorbed PPFD (μmol photon m^{-2} s^{-1}) to which $V_{cmax.gt}$ acclimates, m_c and m are the CO_2 limitation terms for A_C and A_J, respectively, c_i is the leaf-internal partial pressure of CO_2 (Pa), Γ^* is the photorespiratory compensation point (Pa), and K is the effective Michaelis-Menten coefficient of Rubisco (Pa). Optimal stomatal regulation, according to the least-cost hypothesis (*49*), yields the following relationship of c_i to environmental variables, including vapor pressure deficit (D, Pa) and c_a

$$c_i = (\xi c_a + \Gamma^* \sqrt{D})/(\xi + \sqrt{D}) \quad (18)$$

where

$$\xi = \sqrt{[\beta(\Gamma^* + K)/(1.6\eta^*)]} \quad (19)$$

The dimensionless parameter β in Eq. 19 is the ratio of unit costs for the maintenance of carboxylation and water transport capacities, evaluated at 25°C. The term η^* is the viscosity of water (normalized by its value at 25°C), which declines with increasing temperature, thereby reducing the cost of water transport and thereby favoring higher c_i. The value of c_i thus depends on temperature via η^*, Γ^*, and K, as well as on D and c_a (*49*). Analysis of a global leaf stable carbon isotope dataset (*20*) has provided empirical support for the separate dependencies of the c_i:c_a ratio on temperature, vapor pressure deficit, and elevation implied by (Eqs. 18 and 19) and an estimated value of $\beta \approx 146$ (*20*, *50*).

The temperature dependencies of Γ^*, K, and V_{cmax} within normal physiological ranges can be described by the Arrhenius function (*51*) with different activation energies [the formulation for K is somewhat more complex as it depends on the affinities of Rubisco for CO_2 and O_2 and their distinct activation energies, while both Γ^* and K are influenced by atmospheric pressure; see (*51*) for details]. V_{cmax25} is related to $V_{cmax.gt}$ by

$$V_{cmax25} = V_{cmax.gt}/h_T \quad (20)$$

where h_T is the Arrhenius function for V_{cmax}.

We further assume that the coordination hypothesis defines the initial photosynthetic capacity of the leaf. Thus,

$$A_0 = k_1\ k_2\ V_{cmax.gt}\ m_c \quad (21)$$

Here, k_1 and k_2 together convert the unit of $V_{cmax.gt}$ from μmol C m^{-2} s^{-1} into g biomass m^{-2} day^{-1} to match the units of A_0.

Optimal leaf longevity in evergreen species

Substituting Eqs. 12 to 21 into (Eq. 7) yields Eq. 1. Substituting Eq. 7 into Eq. 5 also yields an expression for an evergreen leaf's average daily net carbon gain

$$g_{ev} = f\ A_0\{1 - \sqrt{[2\ C_c/(u\ h_T m_c f)]}\} \quad (22)$$

which is independent of either LMA or LL. In other words, any combination of LMA and LL that satisfies the optimality criterion will yield the same daily net carbon gain. This equivalence may provide a first-order explanation for the large variation in LMA and LL commonly observed within any one plant community.

The coordination hypothesis also relates the initial rate of carbon assimilation to the electron transport–limited photosynthetic rate

$$A_0 = k_1\ \varphi_0\ \Sigma I_{abs}\ m \quad (23)$$

where ΣI_{abs} is the integrated I_{abs} through a day (mol photon m^{-2} day^{-1}). It follows that

$$\mathrm{LL}_{ev} = \mathrm{LMA}\ x_{T.ev} \sqrt{(2u\ C_c/f)/(\Sigma I_{abs}\ k_1)} \quad (24)$$

where

$$x_{T.ev} = \sqrt{(h_T\ m_c)/(\varphi_0 m)} \quad (25)$$

The composite term $x_{T.ev}$ includes the temperature-dependent variables. We express the parameter C_c as a function of LL, LMA, and environmental predictors by rearranging Eqs. 24 and 25 as follows

$$C_c = f(\mathrm{LL}\varphi_0 \Sigma I_{abs}\ m\ k_1/\mathrm{LMA})^2/(2u\ h_T m_c) \quad (26)$$

On the basis of all paired observations of LL and LMA in evergreen species in Glopnet (326 samples), we estimated a median value of C_c = 13.23 ± 4.07 gC gC^{-1} (means ± SE).

Optimality leaf longevity in deciduous species

Substituting Eqs. 12, 15, and 20 into Eq. 11 yields Eq. 2. Substituting Eq. 2 into 9 also yields an expression for a deciduous leaf's average daily net carbon gain

$$g_{de} = f\ A_0[1/2 - C_c/(u\ h_T m_c)] \quad (27)$$

As in evergreen species, g_{de} is independent of either LMA or LL. The different formulae for g_{de} and g_{ev} potentially allow modeling of competition between the two strategies.

Following similar logic to that applied to evergreens, Eq. 23 is then substituted into Eq. 2, leading to a prediction of LL_{de} from LMA and environmental variables

$$LL_{de} = LMA\ u\ x_{T.de}/(\Sigma I_{abs}\ k_1) \quad (28)$$

where

$$x_{T.de} = (h_T\ m_c)/(\varphi_0 m) \quad (29)$$

Linearized models for optimal LL

To facilitate comparisons of data with theoretical predictions, Eq. 24 can be linearized

$$\ln LL_{ev} = \ln LMA - \ln \Sigma I_{abs} - 0.5 \ln f + \ln x_{T.ev} + C_{ev} \quad (30)$$

where

$$C_{ev} = 0.5 \ln (2\ u\ C_c) - \ln k_1 \quad (31)$$

By taking the partial derivative of $\ln x_{T.ev}$ with respect to temperature, we calculated that $LL_{opt.ev}$ increases with growth temperature (T_g, K) by 2.6% K^{-1} under standard environmental conditions. Thus, $\ln x_{T.ev}$ can be replaced by the sum of 0.026 T_g and $\ln x_{T.ev}$ at the reference condition ($\ln x_{T0.ev}$). D and z are also expected to influence LL_{opt} slightly via their effects on optimal c_i, but these effects are too small to be detected.

Similar logic yields a linearized model of LL for deciduous species from Eq. 28

$$\ln LL_{de} = \ln LMA - \ln \Sigma I_{abs} + \ln x_{T.de} + C_{de} \quad (32)$$

where

$$C_{de} = \ln u - \ln k_1 \quad (33)$$

The thermal sensitivity of LL_{de} is twice of that in evergreen species. Thus, $\ln x_{T.de}$ can be replaced by 0.052 T_g plus its reference value ($\ln x_{T0.de}$).

Distributions of evergreen LMA and LL

Different combinations of LMA and LL consistent with the optimality criterion result in equal net carbon gain, implying the existence of a LES along which species with different LMA are equally competitive. Nonetheless, within-site distributions of LMA and LL are known to vary systematically with climate. To account for this variation, it is necessary first to take account of their prior distributions in the species pool. We fitted log-normal distributions to observed LMA and LL data independently in the full Glopnet dataset (fig. S1). Equation 24 was then imposed as a constraint, representing environmental filtering of the species pool. This procedure generates site-specific log-normal distributions, which serve as predictions of the probability density functions of LMA and LL subject to the optimality criterion as illustrated in fig. S2.

Environmental dependencies of LMA

Equation 30 can be reconfigured as an expression for the optimal LMA of evergreen species

$$\ln LMA_{ev} = \ln \Sigma I_{abs} + 0.5 \ln f - 0.026\ T_g + \ln LL_{ev} + C_{ev}' \quad (34)$$

where

$$C_{ev}' = \ln k_1 - 0.5 \ln (2u\ C_c) - \ln x_{T0.ev} \quad (35)$$

Optimal LMA depends on LL and environmental factors. For a given LL, Eq. 34 implies that LMA (all else equal) should increase in proportion to absorbed PPFD and the square root of growing-season length but should decrease with temperature by 2.6% K^{-1}. The prior normal distributions of ln LMA and ln LL, together with their predicted proportional relationship, allow LMA to be predicted from environment alone (fig. S2). Here, we consider ΣI_{abs} as an example to make the derivation, noting that the effects of the other environmental variables (f and T_g) can be derived following the same logic. We specify Eqs. 34 and 35 at two sites with different light conditions (ΣI_1 and ΣI_2) but the same growing-season length and growth temperature. The subscripts "1" and "2" in the equations below distinguish the two sites

$$\ln LMA_{ev1} = \ln \Sigma I_1 + 0.5 \ln f - 0.026\ T_g + \ln LL_{ev1} + C_{ev}' \quad (36)$$

$$\ln LMA_{ev2} = \ln \Sigma I_2 + 0.5 \ln f - 0.026\ T_g + \ln LL_{ev2} + C_{ev}' \quad (37)$$

Thus,

$$\ln LMA_{ev1} - \ln LMA_{ev2} = \ln \Sigma I_1 - \ln \Sigma I_2 + \ln LL_{ev1} - \ln LL_{ev2} \quad (38)$$

The normal distribution constraint induces a line perpendicular to the optimality lines for evergreen species (fig. S2)

$$\ln LL_{ev1} = k - \ln LMA_{ev1} \quad (39)$$

$$\ln LL_{ev2} = k - \ln LMA_{ev2} \quad (40)$$

where k is the intercept of this line. Therefore,

$$\ln LL_{ev1} - \ln LL_{ev2} = \ln LMA_{ev2} - \ln LMA_{ev1} \quad (41)$$

Combining Eqs. 38 and 41 yields

$$\ln LMA_{ev2} - \ln LMA_{ev1} = 0.5(\ln \Sigma I_2 - \ln \Sigma I_1) \quad (42)$$

Similarly, for the growing-season length and temperature

$$\ln LMA_{ev2} - \ln LMA_{ev1} = 0.25\ (\ln f_2 - \ln f_1) \quad (43)$$

$$\ln LMA_{ev2} - \ln LMA_{ev1} = -0.013\ (T_{g2} - T_{g1}) \quad (44)$$

Thus, when moving from site 1 to site 2, the predicted changes in LMA are 50, 25, and −13% of the changes in PPFD, growing-season

length, and temperature respectively. Thus,

$$\ln \mathrm{LMA_{ev}} = 0.25 \ln f + 0.5 \ln \Sigma I_{abs} - 0.013 \; T_g + C_{ev}' \quad (45)$$

As the life span of deciduous leaves is constrained by growing-season length, $\mathrm{LL_{de}}$ should also be proportional to f ($\mathrm{LL_{de}} = 365 f$). Rearranging Eq. 32 and imposing this additional constraint yields the following expression for deciduous LMA as a function of environment alone

$$\ln \mathrm{LMA_{de}} = \ln f + \ln \Sigma I_{abs} - 0.052 \; T_g + C_{de}' \quad (46)$$

where

$$C_{de}' = \ln k_1 + \ln 365 - \ln u - \ln x_{T0,de} \quad (47)$$

Equation 46 implies that deciduous LMA, unlike evergreen LMA, should increase in direct proportion to both PPFD and growing-season length and decline with warming four times faster than in evergreens.

The aridity constraint on LMA

Last, we account for the expected increase in LMA with aridity as an additional constraint on LMA for both deciduous and evergreen species. This constraint could, in principle, have been included in Eqs. 34 and 45 as an independent predictor, but the current optimality framework does not predict the magnitude of this response. We therefore estimated the aridity effect empirically, based on a regression of ln LMA against climatic variables, and used this additional information to modify the predicted latitudinal trends in evergreen and deciduous LMA and the predicted within-site distribution of evergreen LMA, shifting the peak to higher values in drier sites. This estimation was performed on the basis of all LMA observations from Glopnet and CPTD combined to obtain the largest possible sample size. The regression coefficients for light, growing season length, and temperature were fixed at their theoretically predicted values, allowing the effect of aridity alone to be calibrated. Aridity effects on LMA in deciduous and evergreen species were estimated separately (table S4). Estimated aridity effects were included in the predictions of both latitudinal trends and within-site distributions of LMA.

Statistical analysis

Errors-in-variables multiple regression (accounting for measurement errors in predictors and the response variable) was used as the principal approach to estimate partial environmental dependencies of LL and LMA from data, for comparison with independent predictions from theory. This method accounts for uncertainty in each predictor, which we estimated using the coefficient of variation based on interannual climate variability (see the "Site climate data" section above). All traits and bioclimatic variables except for temperature were log-transformed (consistent with the theoretical model, where all variables were log-transformed for the purpose of linearization). We excluded deciduous species from sites with year-round temperatures >0°C, which were presumed to be drought-deciduous. The effect of this exclusion could only be minor, however, as it merely reduces the sample size for deciduous LMA to 292 in Glopnet and 621 in the CPTD.

We first tested the climatic controls of the relationship between LL and LMA using the Glopnet data for evergreens. The constraint of growing-season length on LL in deciduous species was also tested using Glopnet data. We further tested the relationships between LL and LMA by fitting (i) a hierarchical mixed-effects model, including site as a random effect on both the slope and the intercept, and (ii) SMA regressions within individual sites for which sample size was adequate. We then tested the climatic controls on LMA using both Glopnet and CPTD data, but CPTD-based results are given in the main results because of their more reliable bioclimatic data (1-km resolution in CPTD versus 0.5° resolution in Glopnet) and larger sample size, especially for deciduous species (621 in the CPTD versus 292 in Glopnet), in the CPTD. However, Glopnet covers a greater latitudinal range (55°S to 78.93°N in Glopnet versus 28.19°N to 53.47°N in the CPTD), and so Glopnet LMA data were used to analyze latitudinal trends. All statistical analyses were performed in R (version 3.5.2), using the eivtools, 'lmer', and 'smatr' packages.

Global distributions of LL and LMA were derived on the basis of all the samples in Glopnet and site-specific distributions estimated as described above (see the "Environmental dependencies of LMA" section). Six sites from Glopnet with relatively large sample sizes were selected to test the predicted within-site distributions of LMA: two sites each from evergreen-dominant vegetation in tropical rain forests, temperate forests, and woodlands (for details, see table S3). As shown in fig. S2, the global distribution is constrained by the site-specific optimal relationship of ln LL to ln LMA with the slope set to unity and the intercept being the sum of the estimated value of C and the climatic terms in Eq. 30. Predicted distributions of ln LMA were generated after further imposing the aridity effect (see the "The aridity constraint on LMA" section above).

Supplementary Materials

This PDF file includes:

Figs. S1 to S7
Table S1 to S5

REFERENCES AND NOTES

1. M. Westoby, D. Warton, P. B. Reich, The time value of leaf area. *Am. Nat.* **155**, 649–656 (2000).
2. R. M. Deans, T. J. Brodribb, F. A. Busch, G. D. Farquhar, Optimization can provide the fundamental link between leaf photosynthesis, gas exchange and water relations. *Nat. Plants* **6**, 1116–1125 (2020).
3. I. J. Wright, P. B. Reich, M. Westoby, D. D. Ackerly, Z. Baruch, F. Bongers, J. Cavender-Bares, T. Chapin, J. H. C. Cornelissen, M. Diemer, J. Flexas, E. Garnier, P. K. Groom, J. Gulias, K. Hikosaka, B. B. Lamont, T. Lee, W. Lee, C. Lusk, J. J. Midgley, M.-L. Navas, Ü. Niinemets, J. Oleksyn, N. Osada, H. Poorter, P. Poot, L. Prior, V. I. Pyankov, C. Roumet, S. C. Thomas, M. G. Tjoelker, E. J. Veneklaas, R. Villar, The worldwide leaf economics spectrum. *Nature* **428**, 821–827 (2004).
4. P. B. Reich, M. B. Walters, D. S. Ellsworth, From tropics to tundra: Global convergence in plant functioning. *Proc. Natl. Acad. Sci. U.S.A.* **94**, 13730–13734 (1997).
5. E. Cui, K. Huang, M. A. Arain, J. B. Fisher, D. N. Huntzinger, A. Ito, Y. Luo, A. K. Jain, J. Mao, A. M. Michalak, S. Niu, N. C. Parazoo, C. Peng, S. Peng, B. Poulter, D. M. Ricciuto, K. M. Schaefer, C. R. Schwalm, X. Shi, H. Tian, W. Wang, J. Wang, Y. Wei, E. Yan, L. Yan, N. Zeng, Q. Zhu, J. Xia, Vegetation functional properties determine uncertainty of simulated ecosystem productivity: A traceability analysis in the East Asian monsoon region. *Global Biogeochem. Cycles* **33**, 668–689 (2019).
6. N. Carvalhais, M. Forkel, M. Khomik, J. Bellarby, M. Jung, M. Migliavacca, M. μu, S. Saatchi, M. Santoro, M. Thurner, U. Weber, B. Ahrens, C. Beer, A. Cescatti, J. T. Randerson, M. Reichstein, Global covariation of carbon turnover times with climate in terrestrial ecosystems. *Nature* **514**, 213–217 (2014).
7. J. G. Monroe, D. W. Markman, W. S. Beck, A. J. Felton, M. L. Vahsen, Y. Pressler, Ecoevolutionary dynamics of carbon cycling in the Anthropocene. *Trends Ecol. Evol.* **33**, 213–225 (2018).

8. S. Díaz, J. Kattge, J. H. C. Cornelissen, I. J. Wright, S. Lavorel, S. Dray, B. Reu, M. Kleyer, C. Wirth, I. Colin Prentice, E. Garnier, G. Bönisch, M. Westoby, H. Poorter, P. B. Reich, A. T. Moles, J. Dickie, A. N. Gillison, A. E. Zanne, J. Chave, S. Joseph Wright, S. N. Sheremet'ev, H. Jactel, C. Baraloto, B. Cerabolini, S. Pierce, B. Shipley, D. Kirkup, F. Casanoves, J. S. Joswig, A. Günther, V. Falczuk, N. Rüger, M. D. Mahecha, L. D. Gorné, The global spectrum of plant form and function. *Nature* **529**, 167–171 (2016).
9. I. J. Wright, M. Westoby, P. B. Reich, Convergence towards higher leaf mass per area in dry and nutrient-poor habitats has different consequences for leaf life span. *J. Ecol.* **90**, 534–543 (2002).
10. D. S. Falster, P. B. Reich, D. S. Ellsworth, I. J. Wright, M. Westoby, J. Oleksyn, T. D. Lee, Lifetime return on investment increases with leaf lifespan among 10 Australian woodland species. *New Phytol.* **193**, 409–419 (2012).
11. A. van Ommen Kloeke, J. Douma, J. C. Ordoñez, P. B. Reich, P. Van Bodegom, Global quantification of contrasting leaf life span strategies for deciduous and evergreen species in response to environmental conditions. *Glob. Ecol. Biogeogr.* **21**, 224–235 (2012).
12. M. Westoby, D. S. Falster, A. T. Moles, P. A. Vesk, I. J. Wright, Plant ecological strategies: Some leading dimensions of variation between species. *Annu. Rev. Ecol. Evol. Syst.* **33**, 125–159 (2002).
13. J. L. D. Osnas, M. Katabuchi, K. Kitajima, S. J. Wright, P. B. Reich, S. A. van Bael, N. J. B. Kraft, M. J. Samaniego, S. W. Pacala, J. W. Lichstein, Divergent drivers of leaf trait variation within species, among species, and among functional groups. *Proc. Natl. Acad. Sci. U.S.A.* **115**, 5480–5485 (2018).
14. K. Kikuzawa, Y. Onoda, I. J. Wright, P. B. Reich, Mechanisms underlying global temperature-related patterns in leaf longevity. *Glob. Ecol. Biogeogr.* **22**, 982–993 (2013).
15. P. B. Reich, R. L. Rich, X. Lu, Y.-P. Wang, J. Oleksyn, Biogeographic variation in evergreen conifer needle longevity and impacts on boreal forest carbon cycle projections. *Proc. Natl. Acad. Sci. U.S.A.* **111**, 13703–13708 (2014).
16. O. Franklin, S. P. Harrison, R. Dewar, C. E. Farrior, Å. Brännström, U. Dieckmann, S. Pietsch, D. Falster, W. Cramer, M. Loreau, H. Wang, A. Mäkelä, K. T. Rebel, E. Meron, S. J. Schymanski, E. Rovenskaya, B. D. Stocker, S. Zaehle, S. Manzoni, M. van Oijen, I. J. Wright, P. Ciais, P. M. van Bodegom, J. Peñuelas, F. Hofhansl, C. Terrer, N. A. Soudzilovskaia, G. Midgley, I. C. Prentice, Organizing principles for vegetation dynamics. *Nat. Plants* **6**, 444–453 (2020).
17. J. Kattge, G. Bönisch, S. Díaz, S. Lavorel, I. C. Prentice, P. Leadley, S. Tautenhahn, G. D. A. Werner, T. Aakala, M. Abedi, A. T. R. Acosta, G. C. Adamidis, K. Adamson, M. Aiba, C. H. Albert, J. M. Alcántara, C. Alcázar C, I. Aleixo, H. Ali, B. Amiaud, C. Ammer, M. M. Amoroso, M. Anand, C. Anderson, N. Anten, J. Antos, D. M. G. Apgaua, T.-L. Ashman, D. H. Asmara, G. P. Asner, M. Aspinwall, O. Atkin, I. Aubin, L. Baastrup-Spohr, K. Bahalkeh, M. Bahn, T. Baker, W. J. Baker, J. P. Bakker, D. Baldocchi, J. Baltzer, A. Banerjee, A. Baranger, J. Barlow, D. R. Barneche, Z. Baruch, D. Bastianelli, J. Battles, W. Bauerle, M. Bauters, E. Bazzato, M. Beckmann, H. Beeckman, C. Beierkuhnlein, R. Bekker, G. Belfry, M. Belluau, M. Beloiu, R. Benavides, L. Benomar, M. L. Berdugo-Lattke, E. Berenguer, R. Bergamin, J. Bergmann, M. B. Carlucci, L. Berner, M. Bernhardt-Römermann, C. Bigler, A. D. Bjorkman, C. Blackman, C. Blanco, B. Blonder, D. Blumenthal, K. T. Bocanegra-González, P. Boeckx, S. Bohlman, K. Böhning-Gaese, L. Boisvert-Marsh, W. Bond, B. Bond-Lamberty, A. Boom, C. C. F. Boonman, K. Bordin, E. H. Boughton, V. Boukili, D. M. J. S. Bowman, S. Bravo, M. R. Brendel, M. R. Broadley, K. A. Brown, H. Bruelheide, F. Brumnich, H. H. Bruun, D. Bruy, S. W. Buchanan, S. F. Bucher, N. Buchmann, R. Buitenwerf, D. E. Bunker, J. Bürger, S. Burrascano, D. F. R. P. Burslem, B. J. Butterfield, C. Byun, M. Marques, M. C. Scalon, M. Caccianiga, M. Cadotte, M. Cailleret, J. Camac, J. J. Camarero, C. Campany, G. Campetella, J. A. Campos, L. Cano-Arboleda, R. Canullo, M. Carbognani, F. Carvalho, F. Casanoves, B. Castagneyrol, J. A. Catford, J. Cavender-Bares, B. E. L. Cerabolini, M. Cervellini, E. Chacón-Madrigal, K. Chapin, F. S. Chapin, S. Chelli, S.-C. Chen, A. Chen, P. Cherubini, F. Chianucci, B. Choat, K.-S. Chung, M. Chytrý, D. Ciccarelli, L. Coll, C. G. Collins, L. Conti, D. Coomes, J. H. C. Cornelissen, W. K. Cornwell, P. Corona, M. Coyea, J. Craine, D. Craven, J. P. G. M. Cromsigt, A. Csecserits, K. Cufar, M. Cuntz, A. C. da Silva, K. M. Dahlin, M. Dainese, I. Dalke, M. D. Fratte, A. T. Dang-Le, J. Danihelka, M. Dannoura, S. Dawson, A. J. de Beer, A. De Frutos, J. R. De Long, B. Dechant, S. Delagrange, N. Delpierre, G. Derroire, A. S. Dias, M. H. Diaz-Toribio, P. G. Dimitrakopoulos, M. Dobrowolski, D. Doktor, P. Dřevojan, N. Dong, J. Dransfield, S. Dressler, L. Duarte, E. Ducouret, S. Dullinger, W. Durka, R. Duursma, O. Dymova, A. E-Vojtkó, R. L. Eckstein, H. Ejtehadi, J. Elser, T. Emilio, K. Engemann, M. B. Erfanian, A. Erfmeier, A. Esquivel-Muelbert, G. Esser, M. Estiarte, T. F. Domingues, W. F. Fagan, J. Fagúndez, D. S. Falster, Y. Fan, J. Fang, E. Farris, F. Fazlioglu, Y. Feng, F. Fernandez-Mendez, C. Ferrara, J. Ferreira, A. Fidelis, B. Finegan, J. Firn, T. J. Flowers, D. F. B. Flynn, V. Fontana, E. Forey, C. Forgiarini, L. François, M. Frangipani, D. Frank, C. Frenette-Dussault, G. T. Freschet, E. L. Fry, N. M. Fyllas, G. G. Mazzochini, S. Gachet, R. Gallagher, G. Ganade, F. Ganga, P. García-Palacios, V. Gargaglione, E. Garnier, J. L. Garrido, A. L. de Gasper, G. Gea-Izquierdo, D. Gibson, A. N. Gillison, A. Giroldo, M.-C. Glasenhardt, S. Gleason, M. Gliesch, E. Goldberg, B. Göldel, E. Gonzalez-Akre, J. L. Gonzalez-Andujar, A. González-Melo, A. González-Robles, B. J. Graae, E. Granda, S. Graves, W. A. Green, T. Gregor, N. Gross, G. R. Guerin, A. Günther, A. G. Gutiérrez, L. Haddock, A. Haines, J. Hall, A. Hambuckers, W. Han, S. P. Harrison, W. Hattingh, J. E. Hawes, T. He, P. He, J. M. Heberling, A. Helm, S. Hempel, J. Hentschel, B. Hérault, A.-M. Hereş, K. Herz, M. Heuertz, T. Hickler, P. Hietz, P. Higuchi, A. L. Hipp, A. Hirons, M. Hock, J. A. Hogan, K. Holl, O. Honnay, D. Hornstein, E. Hou, N. Hough-Snee, K. A. Hovstad, T. Ichie, B. Igić, E. Illa, M. Isaac, M. Ishihara, L. Ivanov, L. Ivanova, C. M. Iversen, J. Izquierdo, R. B. Jackson, B. Jackson, H. Jactel, A. M. Jagodzinski, U. Jandt, S. Jansen, T. Jenkins, A. Jentsch, J. R. P. Jespersen, G.-F. Jiang, J. L. Johansen, D. Johnson, E. J. Jokela, C. A. Joly, G. J. Jordan, G. S. Joseph, D. Junaedi, R. R. Junker, E. Justes, R. Kabzems, J. Kane, Z. Kaplan, T. Kattenborn, L. Kavelenova, E. Kearsley, A. Kempel, T. Kenzo, A. Kerkhoff, M. I. Khalil, N. L. Kinlock, W. D. Kissling, K. Kitajima, T. Kitzberger, R. Kjøller, T. Klein, M. Kleyer, J. Klimešová, J. Klipel, B. Kloeppel, S. Klotz, J. M. H. Knops, T. Kohyama, F. Koike, J. Kollmann, B. Komac, K. Komatsu, C. König, N. J. B. Kraft, K. Kramer, H. Kreft, I. Kühn, D. Kumarathunge, J. Kuppler, H. Kurokawa, Y. Kurosawa, S. Kuyah, J.-P. Laclau, B. Lafleur, E. Lallai, E. Lamb, A. Lamprecht, D. J. Larkin, D. Laughlin, Y. Le Bagousse-Pinguet, G. le Maire, P. C. le Roux, E. le Roux, T. Lee, F. Lens, S. L. Lewis, B. Lhotsky, Y. Li, X. Li, J. W. Lichstein, M. Liebergesell, J. Y. Lim, Y.-S. Lin, J. C. Linares, C. Liu, D. Liu, U. Liu, S. Livingstone, J. Llusià, M. Lohbeck, Á. López-García, G. Lopez-Gonzalez, Z. Lososová, F. Louault, B. A. Lukács, P. Lukeš, Y. Luo, M. Lussu, S. Ma, C. M. R. Pereira, M. Mack, V. Maire, A. Mäkelä, H. Mäkinen, A. C. M. Malhado, A. Mallik, P. Manning, S. Manzoni, Z. Marchetti, L. Marchino, V. Marcilio-Silva, E. Marcon, M. Marignani, L. Markesteijn, A. Martin, C. Martínez-Garza, J. Martínez-Vilalta, T. Mašková, K. Mason, N. Mason, T. J. Massad, J. Masse, I. Mayrose, J. M. Carthy, M. L. McCormack, K. McCulloh, I. R. McFadden, B. J. McGill, M. Y. McPartland, J. S. Medeiros, B. Medlyn, P. Meerts, Z. Mehrabi, P. Meir, F. P. L. Melo, M. Mencuccini, C. Meredieu, J. Messier, I. Mészáros, J. Metsaranta, S. T. Michaletz, C. Michelaki, S. Migalina, R. Milla, J. E. D. Miller, V. Minden, R. Ming, K. Mokany, A. T. Moles, A. Molnár V, J. Molofsky, M. Molz, R. A. Montgomery, A. Monty, L. Moravcová, A. Moreno-Martínez, M. Moretti, A. S. Mori, S. Mori, D. Morris, J. Morrison, L. Mucina, S. Mueller, C. D. Muir, S. C. Müller, F. Munoz, I. H. Myers-Smith, R. W. Myster, M. Nagano, S. Naidu, A. Narayanan, B. Natesan, L. Negoita, A. S. Nelson, E. L. Neuschulz, J. Ni, G. Niedrist, J. Nieto, Ü. Niinemets, R. Nolan, H. Nottebrock, Y. Nouvellon, A. Novakovskiy; Nutrient Network, K. O. Nystuen, A. O'Grady, K. O'Hara, A. O'Reilly-Nugent, S. Oakley, W. Oberhuber, T. Ohtsuka, R. Oliveira, K. Öllerer, M. E. Olson, V. Onipchenko, Y. Onoda, R. E. Onstein, J. C. Ordonez, N. Osada, I. Ostonen, G. Ottaviani, S. Otto, G. E. Overbeck, W. A. Ozinga, A. T. Pahl, C. E. T. Paine, R. J. Pakeman, A. C. Papageorgiou, E. Parfionova, M. Pärtel, M. Patacca, S. Paula, J. Paule, H. Pauli, J. G. Pausas, B. Peco, J. Penuelas, A. Perea, P. L. Peri, A. C. Petisco-Souza, A. Petraglia, A. M. Petritan, O. L. Phillips, S. Pierce, V. D. Pillar, J. Pisek, A. Pomogaybin, H. Poorter, A. Portsmuth, P. Poschlod, C. Potvin, D. Pounds, A. S. Powell, S. A. Power, A. Prinzing, G. Puglielli, P. Pyšek, V. Raevel, A. Rammig, J. Ransijn, C. A. Ray, P. B. Reich, M. Reichstein, D. E. B. Reid, M. Réjou-Méchain, V. R. de Dios, S. Ribeiro, S. Richardson, K. Riibak, M. C. Rillig, F. Riviera, E. M. R. Robert, S. Roberts, B. Robroek, A. Roddy, A. V. Rodrigues, A. Rogers, E. Rollinson, V. Rolo, C. Römermann, D. Ronzhina, C. Roscher, J. A. Rosell, M. F. Rosenfield, C. Rossi, D. B. Roy, S. Royer-Tardif, N. Rüger, R. Ruiz-Peinado, S. B. Rumpf, G. M. Rusch, M. Ryo, L. Sack, A. Saldaña, B. Salgado-Negret, R. Salguero-Gomez, I. Santa-Regina, A. C. Santacruz-García, J. Santos, J. Sardans, B. Schamp, M. Scherer-Lorenzen, M. Schleuning, B. Schmid, M. Schmidt, S. Schmitt, J. V. Schneider, S. D. Schowanek, J. Schrader, F. Schrodt, B. Schuldt, F. Schurr, G. S. Garvizu, M. Semchenko, C. Seymour, J. C. Sfair, J. M. Sharpe, C. S. Sheppard, S. Sheremetiev, S. Shiodera, B. Shipley, T. A. Shovon, A. Siebenkäs, C. Sierra, V. Silva, M. Silva, T. Sitzia, H. Sjöman, M. Slot, N. G. Smith, D. Sodhi, P. Soltis, D. Soltis, B. Somers, G. Sonnier, M. V. Sørensen, N. A. S. Enio Egon Sosinski Jr., A. F. Souza, M. Spasojevic, M. G. Sperandii, A. B. Stan, J. Stegen, K. Steinbauer, J. G. Stephan, F. Sterck, D. B. Stojanovic, T. Strydom, M. L. Suarez, J.-C. Svenning, I. Svitková, M. Svitok, M. Svoboda, E. Swaine, N. Swenson, M. Tabarelli, K. Takagi, U. Tappeiner, R. Tarifa, S. Tauugourdeau, C. Tavsanoglu, M. T. Beest, L. Tedersoo, N. Thiffault, D. Thom, E. Thomas, K. Thompson, P. E. Thornton, W. Thuiller, L. Tichý, D. Tissue, M. G. Tjoelker, D. Y. P. Tng, J. Tobias, P. Török, T. Tarin, J. M. Torres-Ruiz, B. Tóthmérész, M. Treurnicht, V. Trivellone, F. Trolliet, V. Trotsiuk, J. L. Tsakalos, I. Tsiripidis, N. Tysklind, T. Umehara, V. Usoltsev, M. Vadeboncoeur, J. Vaezi, F. Valladares, J. Vamosi, P. M. van Bodegom, M. van Breugel, E. Van Cleemput, M. van de Weg, S. van der Merwe, F. van der Plas, M. T. van der Sande, M. van Kleunen, K. Van Meerbeek, M. Vanderwel, K. A. Vanselow, A. Vårhammar, L. Varone, M. Y. V. Valderrama, K. Vassilev, M. Vellend, E. J. Veneklaas, H. Verbeeck, K. Verheyen, A. Vibrans, I. Vieira, J. Villacís, C. Violle, P. Vivek, K. Wagner, M. Waldram, A. Waldron, A. P. Walker, M. Waller, G. Walther, H. Wang, F. Wang, W. Wang, H. Watkins, J. Watkins, U. Weber, J. T. Weedon, L. Wei, P. Weigelt, E. Weiher, A. W. Wells, C. Wellstein, E. Wenk, M. Westoby, A. Westwood, P. J. White, M. Whitten, M. Williams, D. E. Winkler, K. Winter, C. Womack, I. J. Wright, S. J. Wright, J. Wright, B. X. Pinho, F. Ximenes, T. Yamada, K. Yamaji, R. Yanai, N. Yankov, B. Yguel, K. J. Zanini, A. E. Zanne, D. Zelený, Y.-P. Zhao, J. Zheng, J. Zheng, K. Ziemińska, C. R. Zirbel, G. Zizka, I. C. Zo-Bi, G. Zotz, C. Wirth, TRY plant trait database – enhanced coverage and open access. *Glob. Chang. Biol.* **26**, 119–188 (2020).
18. S. P. Harrison, W. Cramer, O. Franklin, I. C. Prentice, H. Wang, Å. Brännström, H. Boer, U. Dieckmann, J. Joshi, T. F. Keenan, A. Lavergne, S. Manzoni, G. Mengoli, C. Morfopoulos, J. Peñuelas, S. Pietsch, K. T. Rebel, Y. Ryu, N. G. Smith, B. D. Stocker, I. J. Wright, Eco-evolutionary optimality as a means to improve vegetation and land-surface models. *New Phytol.* **231**, 2125–2141 (2021).

19. M. Detto, X. Xu, Optimal leaf life strategies determine $V_{c,max}$ dynamic during ontogeny. *New Phytol.* **228**, 361–375 (2020).
20. H. Wang, I. C. Prentice, T. F. Keenan, T. W. Davis, I. J. Wright, W. K. Cornwell, B. J. Evans, C. Peng, Towards a universal model for carbon dioxide uptake by plants. *Nat. Plants* **3**, 734–741 (2017).
21. N. Dong, I. C. Prentice, I. J. Wright, B. J. Evans, H. F. Togashi, S. Caddy-Retalic, F. A. McInerney, B. Sparrow, E. Leitch, A. J. Lowe, Components of leaf-trait variation along environmental gradients. *New Phytol.* **228**, 82–94 (2020).
22. K. Kikuzawa, A cost-benefit analysis of leaf habit and leaf longevity of trees and their geographical pattern. *Am. Nat.* **138**, 1250–1263 (1991).
23. X. Xu, D. Medvigy, S. Joseph Wright, K. Kitajima, J. Wu, L. P. Albert, G. A. Martins, S. R. Saleska, S. W. Pacala, Variations of leaf longevity in tropical moist forests predicted by a trait-driven carbon optimality model. *Ecol. Lett.* **20**, 1097–1106 (2017).
24. J.-L. Chen, J. F. Reynolds, P. C. Harley, J. D. Tenhunen, Coordination theory of leaf nitrogen distribution in a canopy. *Oecologia* **93**, 63–69 (1993).
25. A. Haxeltine, I. C. Prentice, A general model for the light-use efficiency of primary production. *Funct. Ecol.* **10**, 551–561 (1996).
26. N. G. Smith, T. F. Keenan, I. Colin Prentice, H. Wang, I. J. Wright, Ü. Niinemets, K. Y. Crous, T. F. Domingues, R. Guerrieri, F. Yoko Ishida, J. Kattge, E. L. Kruger, V. Maire, A. Rogers, S. P. Serbin, L. Tarvainen, H. F. Togashi, P. A. Townsend, M. Wang, L. K. Weerasinghe, S.-X. Zhou, Global photosynthetic capacity is optimized to the environment. *Ecol. Lett.* **22**, 506–517 (2019).
27. T. F. Keenan, Ü. Niinemets, Global leaf trait estimates biased due to plasticity in the shade. *Nat. Plants* **3**, 16201 (2016).
28. P. J. Mitchell, E. J. Veneklaas, H. Lambers, S. S. O. Burgess, Leaf water relations during summer water deficit: Differential responses in turgor maintenance and variation in leaf structure among different plant communities in south-western Australia. *Plant Cell Environ.* **31**, 1791–1802 (2008).
29. S. T. Michaletz, M. D. Weiser, J. Zhou, M. Kaspari, B. R. Helliker, B. J. Enquist, Plant thermoregulation: Energetics, trait–environment interactions, and carbon economics. *Trends Ecol. Evol.* **30**, 714–724 (2015).
30. H. Wang, S. P. Harrison, I. C. Prentice, Y. Yang, F. Bai, H. F. Togashi, M. Wang, S. Zhou, J. Ni, The China plant trait database: Toward a comprehensive regional compilation of functional traits for land plants. *Ecology* **99**, 500 (2018).
31. I. J. Wright, P. B. Reich, J. H. C. Cornelissen, D. S. Falster, P. K. Groom, K. Hikosaka, W. Lee, C. H. Lusk, Ü. Niinemets, J. Oleksyn, N. Osada, H. Poorter, D. I. Warton, M. Westoby, Modulation of leaf economic traits and trait relationships by climate. *Glob. Ecol. Biogeogr.* **14**, 411–421 (2005).
32. D. Sancho-Knapik, A. Escudero, S. Mediavilla, C. Scoffoni, J. Zailaa, J. Cavender-Bares, T. G. Álvarez-Arenas, A. Molins, D. Alonso-Forn, J. P. Ferrio, J. J. Peguero-Pina, E. Gil-Pelegrín, Deciduous and evergreen oaks show contrasting adaptive responses in leaf mass per area across environments. *New Phytol.* **230**, 521–534 (2021).
33. E. Weng, C. E. Farrior, R. Dybzinski, S. W. Pacala, Predicting vegetation type through physiological and environmental interactions with leaf traits: Evergreen and deciduous forests in an earth system modeling framework. *Glob. Change Biol.* **23**, 2482–2498 (2017).
34. L. A. Donovan, H. Maherali, C. M. Caruso, H. Huber, H. de Kroon, The evolution of the worldwide leaf economics spectrum. *Trends Ecol. Evol.* **26**, 88–95 (2011).
35. H. Poorter, Ü. Niinemets, L. Poorter, I. J. Wright, R. Villar, Causes and consequences of variation in leaf mass per area (LMA): A meta-analysis. *New Phytol.* **182**, 565–588 (2009).
36. E. Cui, E. Weng, E. Yan, J. Xia, Robust leaf trait relationships across species under global environmental changes. *Nat. Commun.* **11**, 2999 (2020).
37. N. Dong, I. J. Wright, J. M. Chen, X. Luo, H. Wang, T. F. Keenan, N. G. Smith, I. C. Prentice, Rising CO_2 and warming reduce global canopy demand for nitrogen. *New Phytol.* **235**, 1692–1700 (2022).
38. S. P. Harrison, M. F. Sanchez Goñi, Global patterns of vegetation response to millennial-scale variability and rapid climate change during the last glacial period. *Quat. Sci. Rev.* **29**, 2957–2980 (2010).
39. W. K. Soh, I. J. Wright, K. L. Bacon, T. I. Lenz, M. Steinthorsdottir, A. C. Parnell, J. C. McElwain, Palaeo leaf economics reveal a shift in ecosystem function associated with the end-Triassic mass extinction event. *Nat. Plants* **3**, 17104 (2017).
40. Y. Geng, W. Ma, L. Wang, F. Baumann, P. Kühn, T. Scholten, J.-S. He, Linking above- and belowground traits to soil and climate variables: An integrated database on China's grassland species. *Ecology* **98**, 1471–1471 (2017).
41. T. W. Davis, I. C. Prentice, B. D. Stocker, R. T. Thomas, R. J. Whitley, H. Wang, B. J. Evans, A. V. Gallego-Sala, M. T. Sykes, W. Cramer, Simple process-led algorithms for simulating habitats (SPLASH v. 1.0): Robust indices of radiation, evapotranspiration and plant-available moisture. *Geosci. Model Dev.* **10**, 689–708 (2017).
42. M. New, D. Lister, M. Hulme, I. Makin, A high-resolution data set of surface climate over global land areas. *Climate Res.* **21**, 1–25 (2002).
43. H. Wang, O. K. Atkin, T. F. Keenan, N. G. Smith, I. J. Wright, K. J. Bloomfield, J. Kattge, P. B. Reich, I. C. Prentice, Acclimation of leaf respiration consistent with optimal photosynthetic capacity. *Glob. Chang. Biol.* **26**, 2573–2583 (2020).
44. M. Claverie, E. Vermote, NOAA climate data record (CDR) of leaf area index (LAI) and fraction of absorbed photosynthetically active radiation (FAPAR) version 4. *NOAA National Centers for Environmental Information* **10**, V5M043BX (2014).
45. G. D. Farquhar, S. von Caemmerer, J. A. Berry, A biochemical model of photosynthetic CO_2 assimilation in leaves of C_3 species. *Planta* **149**, 78–90 (1980).
46. G. J. Collatz, J. T. Ball, C. Griveta, J. A. Berry, Physiological and environmental regulation of stomatal conductance, photosynthesis and transpiration: A model that includes a laminar boundary layer. *Agric. For. Meteorol.* **54**, 107–136 (1991).
47. V. Maire, P. Martre, J. Kattge, F. Gastal, G. Esser, S. Fontaine, J. F. Soussana, The coordination of leaf photosynthesis links C and N fluxes in C_3 plant species. *PlOS ONE* **7**, e38345 (2012).
48. C. J. Bernacchi, C. Pimentel, S. P. Long, *In vivo* temperature response functions of parameters required to model RuBP-limited photosynthesis. *Plant Cell Environ.* **26**, 1419–1430 (2003).
49. I. C. Prentice, N. Dong, S. M. Gleason, V. Maire, I. J. Wright, Balancing the costs of carbon gain and water transport: Testing a new theoretical framework for plant functional ecology. *Ecol. Lett.* **17**, 82–91 (2014).
50. B. D. Stocker, H. Wang, N. G. Smith, S. P. Harrison, T. F. Keenan, D. Sandoval, T. Davis, I. C. Prentice, P-model v1.0: An optimality-based light use efficiency model for simulating ecosystem gross primary production. *Geosci. Model Dev.* **13**, 1545–1581 (2020).
51. C. J. Bernacchi, E. L. Singsaas, C. Pimentel, A. R. Portis Jr., S. P. Long, Improved temperature response functions for models of Rubisco-limited photosynthesis. *Plant Cell Environ.* **24**, 253–259 (2001).

Acknowledgments

Funding: This work was supported by National Natural Science Foundation of China 32022052 and 31971495 (H.W.), Tsinghua University Initiative Scientific Research Program 20223080041 (H.W.), Eric and Wendy Schmidt, by recommendation of the Schmidt Futures program (H.W. and I.C.P.), European Union's Horizon 2020 research and innovation program 787203 REALM (I.C.P.), and Australian Research Council DP170103410 (I.C.P. and I.J.W.) and DP220102547 (I.J.W. and H.W.). **Author contributions:** Theory: H.W., I.C.P., X.X., and K.K. Investigation: H.W., I.C.P., S.Q., I.J.W., and J.Z. Visualization: H.W. Writing—original draft: H.W. Writing—review and editing: H.W., I.C.P., I.J.W., D.I.W., X.X., S.Q., J.Z., K.K., and N.C.S. **Competing interests:** The authors declare that they have no competing interests. **Data and materials availability:** The CPTD and the Geng *et al.* trait dataset are public access (doi:10.1002/ecy.2091, doi:10.1002/ecy.2091). The subset of Glopnet dataset used is publicly accessible via figshare (doi:10.6084/m9.figshare.21800153). The code of the SPLASH model is available on an online repository under the GNU Lesser General Public License (https://bitbucket.org/labprentice/splash). All data needed to evaluate the conclusions in the paper are present in the paper and/or the Supplementary Materials.

Submitted 19 June 2022
Accepted 19 December 2022
Published 18 January 2023
10.1126/sciadv.add5667